

Collinear order and chirality-reorientation transition in the Cairo pentagonal magnet $\text{Bi}_4\text{Fe}_5\text{O}_{13}\text{F}$

Alexander A. Tsirlin,^{1,*} Ioannis Rousochatzakis,^{2,†} Dmitry Filimonov,³

Dmitry Batuk,⁴ Matthias Frontzek,⁵ and Artem M. Abakumov^{3,6,‡}

¹Experimental Physics VI, Center for Electronic Correlations and Magnetism, University of Augsburg, 86159 Augsburg, Germany

²School of Physics and Astronomy, University of Minnesota, Minneapolis, Minnesota 55455, USA

³Department of Chemistry, Lomonosov Moscow State University, 119991 Moscow, Russia

⁴EMAT, University of Antwerp, Groenenborgerlaan 171, B-2020 Antwerp, Belgium

⁵Quantum Condensed Matter Division, Oak Ridge National Laboratory, Oak Ridge, TN 37831, USA

⁶Skolkovo Institute of Science and Technology, Nobel str. 3, 143026 Moscow, Russia

Using a combination of neutron diffraction and Mössbauer spectroscopy, we unravel the sequence of magnetic orders observed in the frustrated Cairo pentagonal magnet $\text{Bi}_4\text{Fe}_5\text{O}_{13}\text{F}$. These orders include two orthogonal magnetic structures with opposite vector chiralities, and an intermediate, partly disordered collinear phase. Stabilization of the collinear phase by quantum fluctuations was predicted theoretically, but $\text{Bi}_4\text{Fe}_5\text{O}_{13}\text{F}$ is very far from the relevant parameter regime. Based on *ab initio* band-structure calculations, we propose that the unusual evolution of the ordered states is driven by the strong single-ion anisotropy on the interlayer Fe^{3+} spins, which are located between the Cairo planes. These spins then play a dual role, on one hand mediating the 3D order and on the other driving a reorientation between the two orthogonal configurations having opposite vector chiralities, with the collinear order naturally emerging as an intermediate phase.

Introduction – Frustrated magnets [1–3] host a plethora of remarkable collective phenomena, ranging from topological spin liquids, long-range entanglement and fractionalized excitations [4–10], to emergent electrodynamics and magnetic monopoles [11–13], and even to spin-induced ferroelectricity [14–16]. While the majority of geometrically frustrated magnets are based on spin triangles (or tetrahedra in 3D), pentagon-based magnets, which are far more difficult to implement in real materials [17], are now attracting increasing attention both in theory [18–27] and experiment [28–34].

The main interest so far has been on the Cairo pentagonal lattice, a periodic arrangement of irregular pentagons with two types of sites, one with three-fold and the other with four-fold connectivity (Fig. 1). Cairo-based models host various phases of classical and quantum nature [24], magnetization plateaux [22, 24, 26, 27], and Kosterlitz-Thouless transitions [22]. By now, there are two main realizations of this lattice, $\text{Bi}_2\text{Fe}_4\text{O}_9$ [28–31, 34] and $\text{Bi}_4\text{Fe}_5\text{O}_{13}\text{F}$ [32], although a similar pentagonal topology can be also identified in the multiferroics RMn_2O_5 ($R=\text{Bi}$, Y , or rare-earth) [35–42] that are known for their complex interplay of commensurate and incommensurate magnetic order with ferroelectricity.

The symmetric version of the Cairo Heisenberg model has two exchange couplings, J_{33} and J_{43} (Fig. 1 a). It hosts three phases in the classical limit [24]: a coplanar orthogonal phase (Fig. 1 b), a collinear ferrimagnet, and a mixed phase in between. Quantum fluctuations convert the latter to a non-magnetic and possibly spin-nematic phase for $S=1/2$. Additionally, they introduce another collinear phase for small J_{43}/J_{33} [24]. This phase features collinear *antiferromagnetic* order on all four-fold sites and on half of the three-fold sites, with the remaining half being disordered (Fig. 1 c).

$\text{Bi}_2\text{Fe}_4\text{O}_9$ and $\text{Bi}_4\text{Fe}_5\text{O}_{13}\text{F}$ feature dumbbells of the 4-fold-sites instead of each single 4-fold site on the Cairo lattice. Additionally, the couplings J_{43} and J'_{43} are nonequiva-

lent (Fig. 1), but the classical phase diagram of this extended model is qualitatively the same (Fig. 3). Furthermore, the calculated interactions (reported here and in [25]) place the two compounds nearly on the same spot in the phase diagram, and deep inside the orthogonal phase. Despite this remarkable similarity, the two compounds show qualitatively different behavior. $\text{Bi}_2\text{Fe}_4\text{O}_9$ orders in the anticipated orthogonal state below 238 K, but $\text{Bi}_4\text{Fe}_5\text{O}_{13}\text{F}$, where Cairo planes are interleaved by an additional layer of Fe3 sites, shows three successive transitions at $T_N \simeq 178$ K, $T_2 \simeq 71$ K, and $T_1 \simeq 62$ K [32], with three distinct magnetically ordered states that we refer to as phase I ($T < T_1$), phase II ($T_1 < T < T_2$), and phase III ($T_2 < T < T_N$). Phase I is orthogonal [32], whereas the nature of phases II and III is unknown to date.

In this Letter, we unravel the nature of these phases, and elucidate their origin. Our main findings are:

i) The intermediate phase II is the quantum-mechanical, partially disordered collinear antiferromagnetic phase of Ref. [24] (Fig. 1 e), despite the fact that we are far away from the corresponding region in the phase diagram and despite the large, ‘classical’ spin $S=5/2$.

ii) Phases I and III are both orthogonal, but with opposite vector chiralities $\chi = \pm c$, as defined in Fig. 1 b. Since the two states are degenerate on the level of the isotropic (Heisenberg) model, anisotropy must play a role.

iii) The onset of the collinear phase II coincides with the significant growing of the moment on the interlayer Fe3 sites, which sit between the Cairo planes and normally act to mediate the 3D ordering between the planes, as e.g. in Ref. [44].

The Fe3 spins are absent in $\text{Bi}_2\text{Fe}_4\text{O}_9$ (where neighboring planes couple directly to each other), so the emerging physical picture is that the interlayer Fe3 spins play a vital role for the magnetic order within the Cairo plane. Specifically, the III→II→I transitions can be understood as a reorientation of

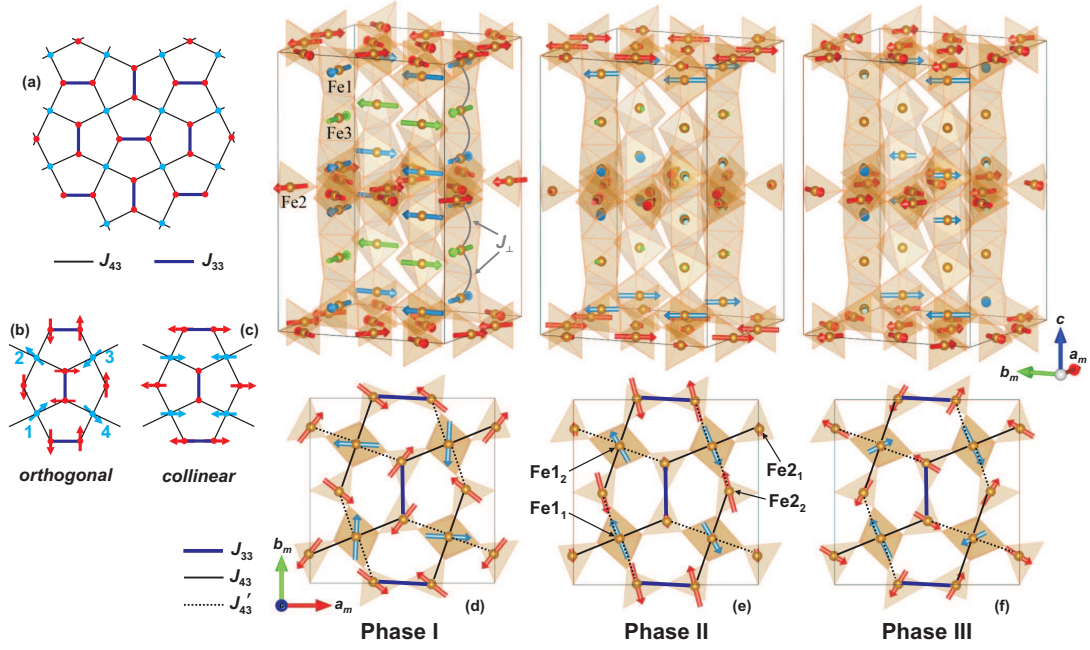


FIG. 1. (a) The symmetric Cairo lattice with two exchange couplings, J_{33} and J_{43} . (b-c) Orthogonal and collinear phases. Note the zero moment on half of the 3-fold sites in (c). The Fe1 sites 1-4 in (b) provide a measure of the chirality as $\chi = \langle \Gamma \rangle / |\langle \Gamma \rangle|$, where $\Gamma = \mathbf{S}_1 \times \mathbf{S}_2 + \mathbf{S}_2 \times \mathbf{S}_3 + \mathbf{S}_3 \times \mathbf{S}_4 + \mathbf{S}_4 \times \mathbf{S}_1$. (d-f) Magnetic structures of $\text{Bi}_4\text{Fe}_5\text{O}_{13}\text{F}$ in phases I, II, and III, respectively. The two types of the J_{43} couplings are also indicated. The crystal and magnetic structures are visualized using VESTA [43].

the nominally preferred orthogonal state, from one orientation (phase III) that satisfies the anisotropy on the in-plane spins to another orientation (phase I) that satisfies the anisotropy on the interlayer Fe3 spins, and in between the system must necessarily go through the collinear phase II.

Neutron powder diffraction – All measurements were performed on single-phase polycrystalline samples of $\text{Bi}_4\text{Fe}_5\text{O}_{13}\text{F}$ prepared previously [32]. Neutron diffraction data were collected at the cold neutron powder diffractometer DMC (LNS PSI, Villigen, Switzerland) with the wavelength of 4.5082 Å in the T range of 1.5–200 K in a He-cryostat. The magnetic structures were refined by the Rietveld method using the JANA2006 program [45]. The symmetry analysis of possible magnetic configurations was carried out in ISODISTORT [46].

Phases I–III share the same propagation vector $\mathbf{k} = (\frac{1}{2}, \frac{1}{2}, 0)$ resulting in a single irrep mM_5^- allowing the moments in the ab plane, similar to $\text{Bi}_2\text{Fe}_4\text{O}_9$. This irrep corresponds to the tetragonal magnetic space group $PC4_2/n$ and the two-fold magnetic supercell defined as: $\mathbf{a}_m = \mathbf{a} - \mathbf{b}$, $\mathbf{b}_m = \mathbf{a} + \mathbf{b}$, $\mathbf{c}_m = \mathbf{c}$. The symmetry implies five nonequivalent Fe positions, as shown in Fig. 1: Fe1₁, Fe1₂, Fe2₁, and Fe2₂ within the Cairo planes and Fe3 between the planes. Fig. 2a shows the size of the magnetic moments as a function of temperature [47].

Phase I (Fig. 1d) is the anticipated orthogonal state, where spins on the Fe1₁ and Fe1₂ sites and on the Fe2₁ and Fe2₂ sites are mutually orthogonal. The ordering along the c direction is locally ferrimagnetic, $\text{Fe1}\uparrow\text{Fe1}\uparrow\text{Fe3}\downarrow\text{Fe1}\uparrow\text{Fe1}\uparrow\text{Fe3}\downarrow$,

but net magnetization is zero, because second-neighbor chains form opposite moments. At 1.5 K, the moments are about $4.0 \mu_B$ on the Fe1 and Fe3 sites and $3.3 \mu_B$ on the Fe2 sites. This difference is due to the stronger Fe–O hybridization for the tetrahedrally coordinated Fe atoms. We note in passing that the magnetic configuration in phase I deviates from our previous report, namely, all spins in the Cairo plane are turned by 90° with respect to Fig. 5 in Ref. [32]. This revised model is based on the better-quality neutron data [47].

As T increases toward T_1 , the Fe1 and Fe2 moments remain roughly unchanged, whereas the moment on Fe3 decreases significantly and drops below $2 \mu_B$ at 55 K. Upon further heating, the magnetic structure changes abruptly entering phase II. All Fe1 sites preserve large moments of 3.2 – $3.8 \mu_B$, whereas the Fe2 sites split into two groups. For Fe2₂, the moments increase to $3.8 \mu_B$, whereas for Fe2₁ they decrease to about $1.2 \mu_B$, only one third of their 1.5 K value. The magnetic structure is nearly collinear and surprisingly similar to the collinear phase predicted for the quantum limit of the Cairo-lattice model [24]. Here, the lower symmetry of the lattice renders J_{43} different from J'_{43} , hence the moment on Fe2₁ does not vanish completely.

The narrow region of phase II is followed by a broader region of phase III, which is again orthogonal, but with opposite vector chirality $\chi = -c$, in contrast to $\chi = +c$ in phase I. In addition, the moments on Fe1₁ are about twice larger than on Fe1₂, whereas the Fe3 moments are too small to be detected experimentally. We obtained $\mu_{\text{Fe3}} = 0.29(25) \mu_B$ at 90 K and, therefore, kept μ_{Fe3} fixed at zero in the final refinement.

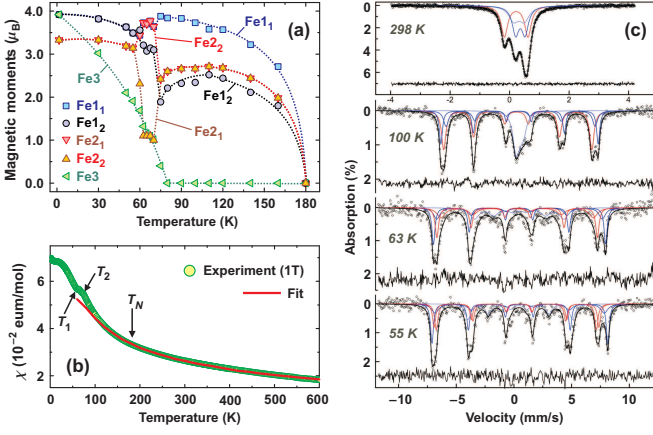


FIG. 2. (a) Temperature dependence of ordered moments obtained from neutron diffraction. Error bars are smaller than the symbol size, lines are guide-for-the-eye only. (b) Fit of the magnetic susceptibility using exchange parameters J_{ij} from DFT. (c) Mössbauer spectra and their fits, as described in the text. For fit parameters, see [47].

Mössbauer spectroscopy – The ^{57}Fe Mössbauer spectra (Fig. 2c) were recorded in the temperature range 55 – 300 K in a transmission mode with a $^{57}\text{Co/Rh}$ γ -ray source using a constant acceleration spectrometer MS1104. At room temperature, the spectrum can be decomposed into 3 doublets with the nearly 40:40:20 ratio of the intensities corresponding to the Fe1, Fe2, and Fe3 positions, respectively [47].

Upon cooling below T_N , the spectra reveal an additional splitting indicative of the magnetic ordering. However, the spectrum at 100 K, in phase III, could not be accounted for by a combination of regular sextets. We found that about 20% of the spectral intensity corresponds to an unresolved sextet with a very weak hyperfine splitting. This signal corresponds to Fe3 that, according to the neutron data, has a very low ordered moment above T_2 . Below T_2 , the Fe3 moments increase and a well-resolved sextet develops, as expected.

The spectrum at 55 K (phase III) contains five magnetic sextets that separate into three groups, Fe1₁ and Fe1₂, Fe2₁ and Fe2₂, and Fe3, as expected from the magnetic structure. The spectrum at 63 K (phase II) is visually quite similar, but one of the Fe2 components is strongly broadened indicating the reduced ordered moment on Fe2₁.

Microscopic description – We begin with the isotropic model defined by the spin Hamiltonian $\mathcal{H} = \sum_{\langle ij \rangle} J_{ij} \mathbf{S}_i \cdot \mathbf{S}_j$, where the summation is over nearest-neighbor spins-5/2, \mathbf{S}_i and \mathbf{S}_j , and J_{ij} are the exchange parameters. Their absolute values are obtained from density-functional (DFT) band-structure calculations performed in the FPLO [48] and VASP [49, 50] codes using the DFT+ U procedure [47]. The couplings were extracted from total energies of collinear spin configurations. In contrast to Ref. [32], they were further refined by fitting experimental magnetic susceptibility with classical Monte-Carlo simulations for the Heisenberg spin model. We find $J_{33} = 116$ K, $J_{43} = 38$ K, and $J'_{43} = 57$ K. The Fe1–Fe3 interaction that mediates the 3D ordering, is $J_{\perp} = 8$ K.

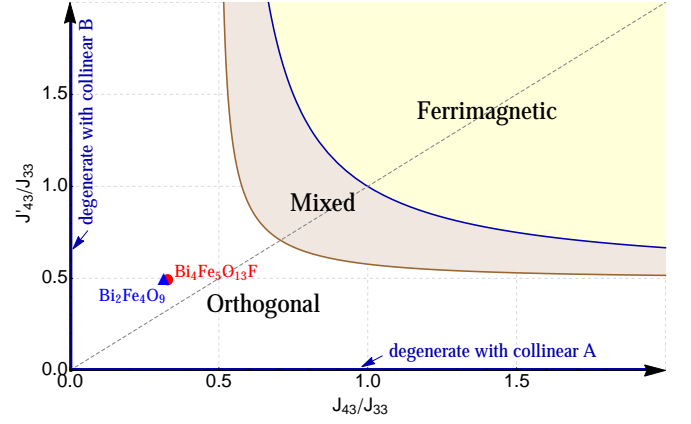


FIG. 3. Classical phase diagram of the Cairo Heisenberg model, with two Fe1–Fe2 couplings, J_{43} and J'_{43} , and two Fe1 spins on each four-fold site of the Cairo lattice, as obtained in [47] using Lyons and Kaplan’s [51] generalization of the Luttinger-Tisza method [52]. The lines $J_{43} = 0$ and $J'_{43} = 0$ correspond to decoupled chains, and the orthogonal phase becomes degenerate with infinite other ground states, including the collinear phases A and B discussed in [47]. The partially disordered collinear phase of [24], which is relevant to phase II of Fig. 1(e), is stabilized by quantum fluctuations in the corner around $J_{43} = J'_{43} = 0$. The line $J_{43} = J'_{43}$ maps to the model of [24] by rescaling $J_{43} \rightarrow J_{43}/2$ and $J'_{43} \rightarrow J'_{43}/2$. The two available compounds are shown by the filled blue triangle (based on the parameters of [25]) and the filled red dot (based on the parameters reported here).

This set of exchange parameters reproduces the susceptibility down to 120 K (Fig. 2b) and predicts $T_N \simeq 180$ K in perfect agreement with the experiment [47].

Our analysis of the isotropic model [47] places $\text{Bi}_4\text{Fe}_5\text{O}_{13}\text{F}$ deep inside the orthogonal phase of the classical phase diagram (Fig. 3). Additionally, the interlayer Fe1–Fe3 coupling is much weaker than the couplings within the plane. Therefore, one expects that the Fe3 spins are more sensitive to thermal fluctuations and decrease much faster than the spins on Fe1 and Fe2 [47], in agreement with Fig. 2a.

Besides these two aspects, the rest of the experimental behavior, including the formation of phases II and III, is completely unexpected on the basis of the isotropic model. First of all, the two phases I and III, which have opposite vector chiralities χ , are degenerate. Second, the system is far away from any collinear phase of the model (Fig. 3), so there is a large energy barrier against any thermally-driven stabilization of collinearity (we have in fact checked and excluded the scenario of thermal stabilization by classical Monte Carlo simulations). Third, the scenario of quantum fluctuations driving the collinear phase is highly unlikely as well: The onset of the collinear phase is roughly taking place when the spin length correction δS from quadratic spin waves approaches the full value $S = 5/2$. According to Fig. 4 of Ref. [24], the collinear phase for $S = 5/2$ (if any) onsets way below $J_{43}/J_{33} = 0.1$, and the actual number should be further divided by two, because here we have two Fe1 sites at each four-fold site. At any

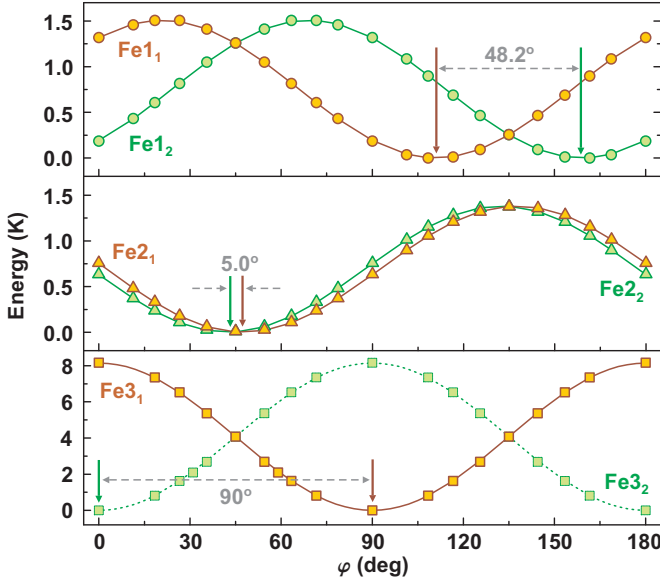


FIG. 4. In-plane single-ion anisotropy energies for the Fe1, Fe2, and Fe3 sites. The arrows denote preferred spin directions. Only the Fe3 sites are compatible with the orthogonal structure, because their preferred directions are at 90° to each other. For the Fe1 and Fe2 sites, the angle between preferred directions of the neighboring sites is largely different from 90° . Note that we use Fe3₁ and Fe3₂ for those Fe3 sites that are coupled to Fe1₁ and Fe1₂, respectively. The angle φ is measured between the magnetic moment and the \mathbf{a}_m -axis, and all curves are periodic, $E(\varphi + 180^\circ) = E(\varphi)$.

rate, our *ab initio* parameters are far away from the stability region of the collinear phase. So phase II is not a thermodynamically stable phase of the isotropic model, but should be thought of as an intermediate step of a reorientation transition from I to III, driven by anisotropy.

Effect of anisotropy – To unravel the origin of this reorientation transition, we must consider anisotropic terms. Dzyaloshinsky-Moriya (DM) couplings are forbidden by symmetry for J_{33} bonds, but are allowed for J_{43} and J'_{43} bonds. However, the analysis of symmetry relations together with the experimental magnetic structures in phases I and III shows that the overall contribution of the c -components of the DM vectors cancels out, hence the DM vectors do not determine the chirality.

In contrast, single-ion anisotropies (Fig. 4) give us the right insights. We first note that the anisotropy of Fe3 is more than 5 times stronger than that of Fe1 and Fe2. Therefore, Fe3 with its preferred directions at $\varphi = 0^\circ$ and 90° puts the Fe1 spins along \mathbf{a}_m and \mathbf{b}_m . This anisotropy does not choose the chirality, but the anisotropy of Fe2 prefers the structure of phase I with $\chi = +c$, as confirmed by a direct energy minimization.

Above T_2 , in phase III, the preferred direction of Fe3 plays no role, and the Fe1 and Fe2 spins are left to form an orthogonal structure, even though their preferred directions do not favor it: for example, the preferred directions of Fe1₁ and Fe1₂ differ by 48.2° only, whereas Fe2₁ and Fe2₂ spins prefer to be nearly collinear. However, deviations from the orthogo-

nal structure are not allowed, because orthogonality is defined by J_{ij} 's, which are at least two orders of magnitude stronger than the anisotropy. This competition between the orthogonal structure and individual single-ion anisotropies explains the unexpected difference in the magnetic moments on the Fe1₁ and Fe1₂ sites in phase III. Indeed, the Fe1₁ moment is larger, because it points approximately along the preferred direction (the departure from the preferred direction is $\Delta\varphi = 5^\circ$ at 100 K). On the other hand, the moment on Fe1₂ is far away from its preferred direction ($\Delta\varphi = 47^\circ$) and thus smaller.

A side effect of these energy considerations is that the chirality changes from $\chi = +c$ in phase I to $\chi = -c$ in phase III. The continuous transformation between these two phases necessitates the intermediate collinear phase II that exists in a narrow temperature range only.

Discussion – The main picture emerging from the experimental data presented here is that the interlayer Fe3 spins in Bi₄Fe₅O₁₃F play a dual role, on one hand mediating the 3D ordering and on the other driving a reorientation of the order in the planes. While details of this transition require further dedicated theoretical work, on the experimental side the effect of the Fe3 spins is crucial for the design of new Cairo-lattice magnets, because interlayer magnetic sites, which are often introduced for the sake of stabilizing the crystal structure [53], are not innocent and in fact play decisive role for the magnetic order within the Cairo planes.

The sequence of transitions in Bi₄Fe₅O₁₃F is closely reminiscent of the consecutive transitions in RMn₂O₅, where an intermediate collinear phase separates two non-collinear states. However, this collinear phase [37] is different from our phase II, because it does not show the characteristic reduction in the ordered moment on part of the (Fe2) sites. Instead, it may be related to the collinear phases A and B of Fig. 3.

Further investigation of the collinear phase II in Bi₄Fe₅O₁₃F would be interesting. For example, an external magnetic field may influence the subtle balance between the two orthogonal states and lead to new partially disordered states resembling phase II. Given the chiral nature of the magnetic structures in phases I and III, detailed investigation of their dielectric properties is also warranted.

Acknowledgment – We are thankful to Prof. J.-M. Perez-Mato for valuable discussion on the magnetic structure. DF and AA are grateful to the Russian Science Foundation (grant 14-13-00680) for support. AT was supported by the Federal Ministry for Education and Research through the Sofja Kovalevskaya Award of Alexander von Humboldt Foundation. This work is based on experiments performed at the Swiss spallation neutron source SINQ, Paul Scherrer Institut, Villigen, Switzerland.

* altsirlin@gmail.com

† irouschoh@umn.edu

‡ A.Abakumov@skoltech.ru

- [1] *Introduction to Frustrated Magnetism: Materials, Experiments, Theory* (Springer Series in Solid-State Sciences, Berlin, 2011).
- [2] *Frustrated Spin Systems*, 2nd ed. (World Scientific, 2013).
- [3] L. Balents, “Spin liquids in frustrated magnets,” *Nature* **464**, 199–208 (2010).
- [4] P.W. Anderson, “Resonating valence bonds: A new kind of insulator?” *Mat. Res. Bull.* **8**, 153 – 160 (1973).
- [5] S. Yan, D. A. Huse, and S. R. White, “Spin-liquid ground state of the $s = 1/2$ kagome Heisenberg antiferromagnet,” *Science* **332**, 1173–1176 (2011).
- [6] S. Depenbrock, I. P. McCulloch, and U. Schollwöck, “Nature of the spin-liquid ground state of the $S = 1/2$ Heisenberg model on the kagome lattice,” *Phys. Rev. Lett.* **109**, 067201 (2012).
- [7] T.-H. Han, J. S. Helton, S. Chu, D. G. Nocera, J. A. Rodriguez-Rivera, C. Broholm, and Y. S. Lee, “Fractionalized excitations in the spin-liquid state of a kagome-lattice antiferromagnet,” *Nature (London)* **492** (2012).
- [8] A. Kitaev, “Anyons in an exactly solved model and beyond,” *Annals of Physics* **321**, 2 – 111 (2006).
- [9] L. Savary and L. Balents, “Quantum spin liquids: a review,” *Rep. Prog. Phys.* **80**, 016502 (2017).
- [10] M. J. P. Gingras and P. A. McClarty, “Quantum spin ice: a search for gapless quantum spin liquids in pyrochlore magnets,” *Rep. Prog. Phys.* **77**, 056501 (2014).
- [11] C. Castelnovo, R. Moessner, and S. L. Sondhi, “Magnetic monopoles in spin ice,” *Nature* **451**, 42–45 (2008).
- [12] C. L. Henley, “The Coulomb phase in frustrated systems,” *Ann. Rev. Condens. Matter Phys.* **1**, 179–210 (2010).
- [13] J. Rehn and R. Moessner, “Maxwell electromagnetism as an emergent phenomenon in condensed matter,” *Phil. Trans. Royal Soc. London A* **374** (2016), 10.1098/rsta.2016.0093.
- [14] S.-W. Cheong and M. Mostovoy, “Multiferroics: a magnetic twist for ferroelectricity,” *Nature Materials* **6**, 13–20 (2007).
- [15] T. Arima, “Spin-driven ferroelectricity and magneto-electric effects in frustrated magnetic systems,” *J. Phys. Soc. Jpn.* **80**, 052001 (2011).
- [16] Y. Tokura, S. Seki, and N. Nagaosa, “Multiferroics of spin origin,” *Rep. Prog. Phys.* **77**, 076501 (2014).
- [17] This is mostly because of the well-known incompatibility of the five-fold symmetry with lattice periodicity.
- [18] R. Moessner and S. L. Sondhi, “Ising models of quantum frustration,” *Phys. Rev. B* **63**, 224401 (2001).
- [19] V. Urumov, “Exact solution of the Ising model on a pentagonal lattice,” *J. Phys. A* **35**, 7317 (2002).
- [20] K. S. Raman, R. Moessner, and S. L. Sondhi, “SU(2)-invariant spin- $\frac{1}{2}$ Hamiltonians with resonating and other valence bond phases,” *Phys. Rev. B* **72**, 064413 (2005).
- [21] A. Jagannathan, B. Motz, and E. Vedmedenko, “Novel properties of frustrated low-dimensional magnets with pentagonal symmetry,” *Phil. Mag.* **91**, 2765–2772 (2011).
- [22] A. Ralko, “Phase diagram of the Cairo pentagonal XXZ spin- $\frac{1}{2}$ magnet under a magnetic field,” *Phys. Rev. B* **84**, 184434 (2011).
- [23] M. Rojas, O. Rojas, and S. M. de Souza, “Frustrated Ising model on the Cairo pentagonal lattice,” *Phys. Rev. E* **86**, 051116 (2012).
- [24] I. Rousochatzakis, A. M. Läuchli, and R. Moessner, “Quantum magnetism on the Cairo pentagonal lattice,” *Phys. Rev. B* **85**, 104415 (2012).
- [25] Z. V. Pchelkina and S. V. Streltsov, “*Ab initio* investigation of the exchange interactions in $\text{Bi}_2\text{Fe}_4\text{O}_9$: The Cairo pentagonal lattice compound,” *Phys. Rev. B* **88**, 054424 (2013).
- [26] H. Nakano, M. Isoda, and T. Sakai, “Magnetization process of the $S = 1/2$ Heisenberg antiferromagnet on the Cairo pentagon lattice,” *J. Phys. Soc. Jpn.* **83**, 053702 (2014).
- [27] M. Isoda, H. Nakano, and T. Sakai, “Frustration-induced magnetic properties of the spin- $1/2$ Heisenberg antiferromagnet on the Cairo pentagon lattice,” *J. Phys. Soc. Jpn.* **83**, 084710 (2014).
- [28] N. Shamir, E. Gurewitz, and H. Shaked, “The magnetic structure of $\text{Bi}_2\text{Fe}_4\text{O}_9$ – analysis of neutron diffraction measurements,” *Acta Cryst.* **A34**, 662–666 (1978).
- [29] A. K. Singh, S. D. Kaushik, B. Kumar, P. K. Mishra, A. Venimadhav, V. Siruguri, and S. Patnaik, “Substantial magnetoelectric coupling near room temperature in $\text{Bi}_2\text{Fe}_4\text{O}_9$,” *Appl. Phys. Lett.* **92**, 132910 (2008).
- [30] E. Ressouche, V. Simonet, B. Canals, M. Gospodinov, and V. Skumryev, “Magnetic frustration in an iron-based Cairo pentagonal lattice,” *Phys. Rev. Lett.* **103**, 267204 (2009).
- [31] M. N. Iliev, A. P. Litvinchuk, V. G. Hadjiev, M. M. Gospodinov, V. Skumryev, and E. Ressouche, “Phonon and magnon scattering of antiferromagnetic $\text{Bi}_2\text{Fe}_4\text{O}_9$,” *Phys. Rev. B* **81**, 024302 (2010).
- [32] A. M. Abakumov, D. Batuk, A. A. Tsirlin, C. Prescher, L. Dubrovinsky, D. V. Sheptyakov, W. Schnelle, J. Hadermann, and G. Van Tendeloo, “Frustrated pentagonal Cairo lattice in the non-collinear antiferromagnet $\text{Bi}_4\text{Fe}_5\text{O}_{13}\text{F}$,” *Phys. Rev. B* **87**, 024423 (2013).
- [33] M. G. Rozova, V. V. Grigoriev, I. A. Bobrikov, D. S. Filimonov, K. V. Zakharov, O. S. Volkova, A. N. Vasiliev, E. V. Antipov, A. A. Tsirlin, and A. M. Abakumov, “Synthesis, structure and magnetic ordering of the mullite-type $\text{Bi}_2\text{Fe}_{4-x}\text{Cr}_x\text{O}_9$ solid solutions with a frustrated pentagonal Cairo lattice,” *Dalton Trans.* **45**, 1192–1200 (2016).
- [34] S. R. Mohapatra, A. Swain, C. S. Yadav, S. D. Kaushik, and A. K. Singh, “Unequivocal evidence of enhanced magnetodielectric coupling in Gd^{3+} substituted multiferroic $\text{Bi}_2\text{Fe}_4\text{O}_9$,” *RSC Adv.* **6**, 112282–112291 (2016).
- [35] K. Saito and K. Kohn, “Magnetoelectric effect and low-temperature phase transitions of TbMn_2O_5 ,” *J. Phys.: Condens. Matter* **7**, 2855 (1995).
- [36] N. Hur, S. Park, P. A. Sharma, J. S. Ahn, S. Guha, and S.-W. Cheong, “Electric polarization reversal and memory in a multiferroic material induced by magnetic fields,” *Nature* **429**, 392 (2004).
- [37] G. R. Blake, L. C. Chapon, P. G. Radaelli, S. Park, N. Hur, S.-W. Cheong, and J. Rodríguez-Carvajal, “Spin structure and magnetic frustration in multiferroic RMn_2O_5 ($R = \text{Tb}, \text{Ho}, \text{Dy}$),” *Phys. Rev. B* **71**, 214402 (2005).
- [38] C. Vecchini, L. C. Chapon, P. J. Brown, T. Chatterji, S. Park, S.-W. Cheong, and P. G. Radaelli, “Commensurate magnetic structures of RMn_2O_5 ($R = \text{Y}, \text{Ho}, \text{Bi}$) determined by single-crystal neutron diffraction,” *Phys. Rev. B* **77**, 134434 (2008).
- [39] A. B. Harris, A. Aharony, and O. Entin-Wohlman, “Order parameters and phase diagram of multiferroic RMn_2O_5 ,” *Phys. Rev. Lett.* **100**, 217202 (2008).
- [40] A. B. Sushkov, M. Mostovoy, R. Valdés Aguilar, S.-W. Cheong, and H. D. Drew, “Electromagnons in multiferroic RMn_2O_5 compounds and their microscopic origin,” *J. Phys.: Condens. Matter* **20**, 434210 (2008).
- [41] J. W. Kim, S. Y. Haam, Y. S. Oh, S. Park, S.-W. Cheong, P. A. Sharma, M. Jaime, N. Harrison, Jung Hoon Han, G.-S. Jeon, P. Coleman, and K. H. Kim, “Observation of a multiferroic critical end point,” *PNAS* **106**, 15573–15576 (2009).
- [42] K. Cao, G.-C. Guo, D. Vanderbilt, and L. He, “First-principles modeling of multiferroic RMn_2O_5 ,” *Phys. Rev. Lett.* **103**, 257201 (2009).

- [43] K. Momma and F. Izumi, “VESTA 3 for three-dimensional visualization of crystal, volumetric and morphology data,” *J. Appl. Crystallogr.* **44**, 1272–1276 (2011).
- [44] R. Nath, K. M. Ranjith, J. Sichelschmidt, M. Baenitz, Y. Skourski, F. Alet, I. Rousochatzakis, and A. A. Tsirlin, “Hindered magnetic order from mixed dimensionalities in CuP_2O_6 ,” *Phys. Rev. B* **89**, 014407 (2014).
- [45] V. Petříček, M. Dušek, and L. Palatinus, “Crystallographic computing system JANA2006: General features,” *Z. Krist.* **229**, 345–352 (2014).
- [46] B. J. Campbell, H. T. Stokes, D. E. Tanner, and D. M. Hatch, “ISODISPLACE: a web-based tool for exploring structural distortions,” *J. Appl. Cryst.* **39**, 607–614 (2006).
- [47] See Supplemental material at [...] for: i) Neutron diffraction patterns and details of the refinement; ii) fitting parameters for the Mössbauer spectra; iii) details of electronic structure calculations; iv) Details on the derivation of the phase diagram presented in Fig. 3; v) Theoretical evidence for the qualitatively different T -dependence of the $\text{Fe}3$ and $\text{Fe}1/\text{Fe}2$ moments.
- [48] K. Koepernik and H. Eschrig, “Full-potential nonorthogonal local-orbital minimum-basis band-structure scheme,” *Phys. Rev. B* **59**, 1743–1757 (1999).
- [49] G. Kresse and J. Furthmüller, “Efficiency of ab-initio total energy calculations for metals and semiconductors using a plane-wave basis set,” *Computational Materials Science* **6**, 15 – 50 (1996).
- [50] G. Kresse and J. Furthmüller, “Efficient iterative schemes for *ab initio* total-energy calculations using a plane-wave basis set,” *Phys. Rev. B* **54**, 11169–11186 (1996).
- [51] D. H. Lyons and T. A. Kaplan, “Method for determining ground-state spin configurations,” *Phys. Rev.* **120**, 1580–1585 (1960); T. A. Kaplan and N. Menyuk, “Spin ordering in three-dimensional crystals with strong competing exchange interactions,” *Phil. Mag.* **87**, 3711–2785 (2007).
- [52] J. M. Luttinger and L. Tisza, “Theory of dipole interaction in crystals,” *Phys. Rev.* **70**, 954–964 (1946).
- [53] J. Cumby, R. D. Bayliss, F. J. Berry, and C. Greaves, “Synthetic analogues of Fe(II) – Fe(III) minerals containing a pentagonal ‘Cairo’ magnetic lattice,” *Dalton Trans.* **45**, 11801–11806 (2016).